A new interpretation of mode I interlaminar fracture in layered materials

Adamos, Lucas; Alderliesten, René; Loutas, Theodoros

DOI
10.1016/j.engfracmech.2024.110400

Publication date
2024

Document Version
Final published version

Published in
Engineering Fracture Mechanics

Engineering Fracture Mechanics 309 (2024) 110400

Contents lists available at ScienceDirect

Engineering Fracture Mechanics

journal homepage: www.elsevier.com/locate/engfracmech

A new interpretation of mode I interlaminar fracture in layered materials

Lucas Adamos [a], René Alderliesten [b,*], Theodoros Loutas [a,*]

[a] *Laboratory of Applied Mechanics and Vibrations, Department of Mechanical Engineering and Aeronautics, University of Patras, GR-26504 Rio-Patras, Greece*

[b] *Aerospace Structures and Materials Department, Faculty of Aerospace Engineering, Delft University of Technology, P.O. Box 5058, 2600 GB Delft, the Netherlands*

A R T I C L E I N F O

Keywords:
Mode-I delamination
Fatigue
Fracture toughness
Fiber bridging
Rate effect

A B S T R A C T

Interlaminar crack propagation in layered materials, such as composites, is still a not fully understood phenomenon in fracture mechanics. Experimental observations reveal a broad spectrum of crack propagation velocities during the interlaminar fracture of layered materials under varying loading conditions and rates. While there have been numerous studies examining interlaminar crack propagation under quasi-static, fatigue, and more recently, high-speed loading, there has been a notable lack of endeavors to present and interpret crack growth data within a unified framework. To this direction, we present a new interpretation of interlaminar crack propagation data acquired from a broad test campaign under various mode-I loading conditions (quasi-static, fatigue and high-speed). We connect the crack tip velocity to the rate of change of the SERR to propose a new equation/model that shows potential in presenting and explaining the variety of experimental crack growth data. This correlation arises from a simple mathematical analysis of the rate of change of the SERR using the chain differentiation rule. Subsequently, it is further substantiated by experimental evidence, in an effort to accommodate results from various experiments under a unified description. A robust correlation of the test data is established through a range of slopes which are proven -experimentally- to be characteristic constants of the mode-I interlaminar fracture of a specific material system.

1. Introduction

Structures that are designed and operated following the damage tolerance philosophy e.g. aerospace structures, acknowledge to an extent the presence and potential evolution of flaws. The application of fracture mechanics principles aims to predict the propagation of cracks in materials and structures. In general, cracks evolve and propagate under a diverse possible spectrum of loading rates, encompassing both monotonic and alternating loading conditions. Until the present day, the engineering community relies on the Paris-Erdogan empirical equation [1,2] originally proposed in the early 1960s to assess the crack propagation in metals. To predict the behavior of delaminated composites under repetitive loading, Paris-like equations [3–10] have been employed that, instead of the stress intensity factor (SIF), K, utilize the strain energy release rate (SERR), G. Paris' and Paris-like approaches use fitting of datapoints and normalization of parameters [6–8,11–14] that lack physical explanation, as criticized in the literature [9,15–17]. Although this

* Corresponding authors.
E-mail addresses: R.C.Alderliesten@tudelft.nl (R. Alderliesten), thloutas@upatras.gr (T. Loutas).

https://doi.org/10.1016/j.engfracmech.2024.110400
Received 21 May 2024; Received in revised form 30 July 2024; Accepted 13 August 2024
Available online 14 August 2024

Nomenclature

a	propagated crack length after the first step of the DCB experiment (mm)
A	crack surface (mm^2)
B	fitting parameter of Paris relationship
b	specimen width (mm)
C	compliance (mm/N)
c^*	stress terms related to fracture behavior (N/mm^2)
D_i	bending stiffness of sub-laminate i, i=1, 2 ($1/Nmm$)
da/dN	fatigue crack growth rate ($mm/cycle$)
$da/dt, \dot{a}$	velocity of the crack tip (mm/s)
$dG/dt, \dot{G}$	rate of change of the SERR (N/mms)
G	total SERR (N/mm)
G_{max}	maximum SERR recorded in each cycle (N/mm)
G_{min}	minimum SERR recorded in each cycle (N/mm)
ΔG	difference between maximum and minimum SERR recorded in each cycle (N/mm)
$\Delta\sqrt{G}$	$= (\sqrt{\mathrm{G}_{\max}} - \sqrt{\mathrm{G}_{\min}})^2$
G^*	physical SERR or resistance to crack growth (N/mm)
h_i	thickness of the sub-laminate i, i=1, 2 (mm)
m	fitting parameter of Paris relationship
N	number of cycles
R	stress ratio
U	potential elastic strain energy stored in the system (J, Nmm)
$v, \dot{\delta}$	loading rate (mm/s)
δ_{max}	maximum deflection at each cycle (mm)
δ_{crit}	critical deflection at each crack length (mm)

Abbreviations

AOR	alternating opening rate(s)
COR	constant opening rate(s)
CFRP	carbon fiber reinforced plastic
DCB	double cantilever beam
GFRP	glass fiber reinforced plastic
SERR	strain energy release rate(s)

relationship successfully describes the experimental data under specific loading rate, due to its empirical nature it fails to provide a unifying framework that diminishes effects discussed extensively in literature [18–25] such as the stress ratio influence. The Hartman-Schijve variation of the Paris relation is considerably more successful in dealing with the stress ratio effect [4,5,19] however it involves the fitting of one more parameter and also asks for the determination of a threshold value of the SERR, a value that is inconsistent in cases where the stress ratio or bridging effect is present. Undoubtedly the Paris relation and its variations are purely phenomenological, an attempt to conditionally explain experimental evidence, rather than a physical law. In the field of interlaminar fracture mechanics, there is a notable absence of equations derived directly from physical principles that predict the velocity of the crack tip of a given material. There is also an ongoing discussion on the appropriate parameter utilized for applying similitude. The Paris-like relation for layered materials, shown in its basic form as

$$\frac{da}{dN} = Bf(G)^m \tag{1}$$

tries to associate the rate of crack growth da/dN under cyclic loading with a function of the SERR. B, m values are determined after least squares regression. The $f(G)$ notation corresponds to the utilization of either G_{max}, ΔG or $\Delta\sqrt{G}$ as similitude parameter which is currently open to the researcher's preference. Alderliesten [16] took a step towards this direction proposing as a similitude parameter the physical strain energy dissipation or applied work, and revealed strong linear correlations between the energy dissipation per cycle and the crack growth rate in mode-I interlaminar fatigue tests. This correlation has been mainly explored under fatigue loading with few notable exceptions [26,27]. Towards a better understanding of this correlation we employ similar analysis expanding the outcomes of previous findings [16,17,26–33].

The hypothesis of the present study posits that interlaminar fracture behavior of materials under various loading conditions (i.e. quasi-static, fatigue, high-speed) may hold shared characteristics, which, as of now, remain undiscovered. The limitation arises from our current approach to examining and plotting results, guided by phenomenological relations -variations of the Paris law- that fall short of revealing a unified interpretation of the interlaminar fracture behavior in layered materials. We find that the method of applying loading rate is a crucial parameter governing the interlaminar fracture of materials. Consequently, we assert that the velocity of the crack tip in a given material is not arbitrary; instead, interlaminar cracks propagate within a specific range of velocities strongly correlated with the imposition of the loading rate. Initially, this correlation arises from a simple mathematical analysis of the rate of change of the SERR using the chain differentiation rule. However, it is subsequently supported with strong experimental evidence. Specimens from Carbon Fiber Reinforced Polymers (CFRP) are tested under the entire spectrum of loading conditions i.e. quasi-static, high-speed and fatigue, utilizing a wide variety of experimental conditions i.e. loading rate ($\dot{\delta}$), frequency (f) and stress ratio (R) combinations. Also, data from Glass Fiber Reinforced Polymers (GFRP) specimens tested under quasi-static and high-speed loading are utilized from the relevant literature [26,34] to verify our proposition in another material system.

2. Materials and methods

2.1. Materials

Two types of materials specimens are utilized for the present study, i.e. CFRP and GFRP composite laminates. The CFRP laminates were produced by hand-lay-up of 32 unidirectional carbon/epoxy prepreg layers of M30SC/DT120, a high strength and modulus carbon fiber/toughed thermosetting epoxy, achieving a nominal cured thickness of 4.8 *mm*. A 12.7 *mm* Teflon film was inserted in the middle plane of the composite laminates to act as an initial delamination. The laminates were cured in vacuum in an autoclave at a pressure of 6 bars and curing temperature of $120^{\circ}\ C$ for 90 *min*. The plate was cut by a diamond saw into 25 *mm* width beams with 250 *mm* length which fulfill the ASTM D5528 requirements. From the plate, specimens were cut and then tabs were bonded on them.

The GFRP composite laminates were produced by hand-lay-up of 24 unidirectional layers of E-glass fibers and a bisphenol A/epichlorohydrin derived liquid epoxy resin with the commercial name of Razeen® LR 1100 hardened with Epikure 3234 by 100:13 wt ratio. A 20 μm Teflon film was inserted in the middle plane of the composite laminates to act as an initial delamination. The laminates were cured at room temperature for 2 days followed by a post-cure scheme of 1 *h* at $80^{\circ} C$ and 2 *h* at $110^{\circ} C$. The plates were cut by a diamond saw into 25 *mm* width beams with 250 *mm* length which fulfill the ASTM D5528 requirements. A pair of Aluminum blocks, 25 *mm* width by 20 *mm* length with 6 *mm* thickness, was adhesively bonded to all specimen's ends to enable the load introduction.

2.2. Experimental procedures

As outlined in Section 1, the method of applying the loading rate is a key parameter of the present study. The experimental campaign presented in this work encompasses quasi-static, high-speed, and fatigue tests. These tests fall into two categories based on

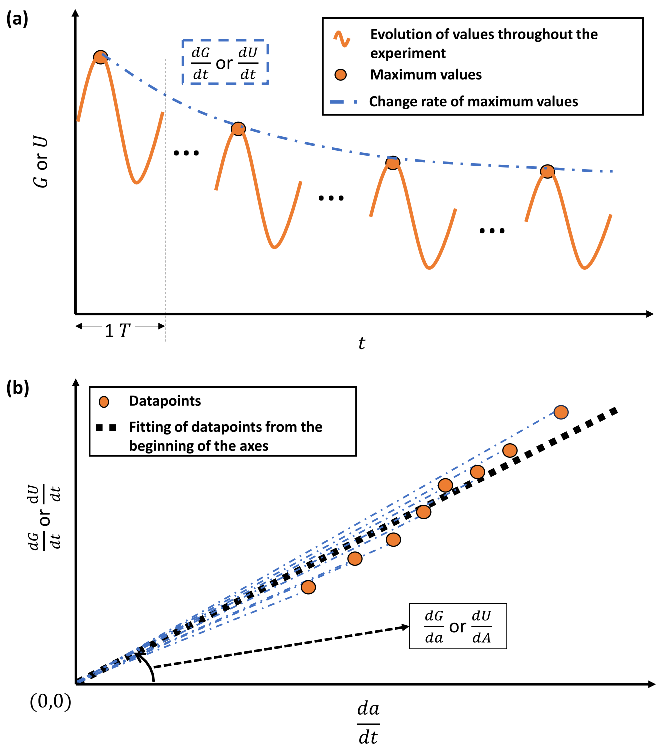

Fig. 1. (a) Evolution of strain energy and SERR values throughout fatigue experiments, (b) determination of the slopes measured from the beginning of the axes. fatigue hysteresis loops extracted from experiments conducted under the two R-ratios used.

the method used to impose the loading rate on the specimens through the testing machine. Quasi-static and high-speed tests share a constant value of opening (or displacement) rate. Therefore, we categorize these tests as Constant Opening Rate (COR) tests, describing the monotonic nature of this loading approach. On the other hand, fatigue tests involve a cyclic or alternating loading rate. Therefore, we categorize fatigue loading as Alternating Opening Rate (AOR) testing. Calculating the parameters under investigation involves time differentiation, which in the case of COR testing is a straightforward procedure, as all data extracted from the machine correspond to the same time derivative. The cyclic nature of fatigue testing influences the evolution of parameters like strain energy and SERR in an oscillatory manner, as depicted in Fig. 1a. Here we calculate both strain energy dissipation and the change in rate of the SERR at the maximum values achieved within the load cycles. Both these parameters are later correlated to the velocity of the crack tip as illustrated in Fig. 1b. This approach facilitates a straightforward comparison with the COR counterparts, where the maximum strain energy is consistently attained.

2.2.1. Constant opening rate (COR) testing

Constant opening rate (COR) datasets of the CFRP and GFRP material systems were obtained from previous works [26,34–36]. DCB tests were conducted following the ASTM D5528 standard on a 15 kN servo-hydraulic machine equipped with a high precision 1 kN Load cell. CFRP tests were performed under displacement control with the applied displacement rate varying from 0.016 mm/s for quasi-static up to 400 mm/s for high-speed testing. GFRP tests were also performed under displacement control with the applied displacement rate varying from 0.016 mm/s up to 200 mm/s. The applied load and displacement were duly recorded. A digital camera and computer system was used to monitor the crack evolution by automatically recording images of the specimen edge. For the quasi-static rates of 0.016 mm/s, a 5 MP digital camera with an 80 mm lens and maximum frequency of 200 Hz recording speed was used. For the rates up to 100 mm/s to facilitate synchronization, the load and displacement signals are sent from the control unit of the test machine as inputs to the camera control system. For the tests performed at 100 mm/s and 400 mm/s, a camera with 120 mm lens was used at 1000 Hz and 2000 Hz respectively and the camera control system was triggered by the control unit of the test machine.

2.2.2. Alternating opening rate (AOR) testing

Alternating opening rate (AOR) testing was conducted using constant amplitude fatigue experiments specifically for the CFRP material. In total 18 fatigue experiments were conducted on CFRP specimens, under two stress ratios, meaning the ratio between the minimum and maximum displacement applied ($R = \delta_{min}/\delta_{max}$), i.e., 0.2 and 0.8. The frequency ranged from 1-5 Hz, such that with corresponding stress ratios, loading rates could be correlated. Prior to the fatigue test, a quasi-static test was conducted for each specimen where the maximum value of displacement δ_{max} that marks the crack initiation point was defined. After completion of the first fatigue test, the specimen was dismounted, and a second static load cycle was conducted to determine the next fatigue experiment's maximum deflection, δ_{max}. Then, the next fatigue experiment started, with a different initial crack length. Each fatigue experiment is terminated upon reaching a plateau in the crack length versus number of cycles graph. Prior to the tests, one side of each specimen was painted white through-the-width, to enhance the visibility of the propagating crack during the tests. The crack length is being monitored through a digital camera pointed at the specimen's side. Every specific number of cycles the experiment pauses, the specimen is loaded up to the maximum deflection, the camera captures the image, and the experiment resumes.

2.3. Theoretical framework

Interlaminar crack propagation under quasi-static or high-speed loading has been studied rather separately and without any attempt to put the experimental findings under a unified framework -if possible- with those from fatigue tests. During fracture experiments conducted under the three aforementioned cases, a broad spectrum of SERR values is obtained even when employing identical specimens. On the other hand, literature has given limited attention to the rate of change of the SERR, $\dot{G}$ [37,38]. Determination of $\dot{G}$ can be achieved through fitting experimental SERR values over time, followed by differentiating the derived equation, so it is necessary to first calculate the SERR itself. In the datasets collected for the present study, measurements of force P, deflection δ, crack length a and time t, were available. We employ the Simple Beam Theory (SBT) formulation of the SERR, as represented by

$$G = \frac{nP\delta}{2ba} \tag{2}$$

where $n = 3$ for the Double Cantilever Beam (DCB) case, P the applied force, δ the deflection of the specimen's arm, b the width of the specimen and a the measured crack length that also includes Δ, the Williams correction factor accounting for the root rotation of the crack tip [39–43]. Minor differences were observed in the results if a higher order theory such as First Order Shear Deformation theory is utilized.

Nevertheless, the applied force P, and the deflection δ, are related by the specimen compliance, $C = \delta/P$. In the framework of the SBT, the compliance as a function of the crack length is expressed as:

$$C = \frac{2a^3}{3D_1} \tag{3}$$

where $D_i = \frac{E_{11}^i b h_i^3}{12}$, the bending stiffness, h_i the thickness and E_{11}^i the longitudinal Young's modulus of the sub laminate i. By introducing Eq. (3) into Eq. (2) the SERR is simply given as:

$$G = \frac{12P^2a^2}{E_{11}b^2h^3} \tag{4}$$

The resulting SERR, as presented in Eq. (4), can be deconstructed as follows:

$$\frac{dG}{dt} = \frac{\partial G}{\partial a}\frac{da}{dt} + \frac{\partial G}{\partial P}\frac{dP}{dt} \Rightarrow \dot{G} = \frac{\partial G}{\partial a}\dot{a} + \frac{\partial G}{\partial P}\dot{P} \tag{5}$$

It is essential to note that the terms derived from this chain differentiation rely on the specific formulation of the SERR. The partial derivatives of the SERR regarding the crack length a, and applied force P, can be extracted from Eq. (4) as follows:

$$\frac{\partial G}{\partial a} = \frac{24P^2a}{E_{11}b^2h^3} = \frac{2G}{a} \tag{6a}$$

$$\frac{\partial G}{\partial P} = \frac{24Pa^2}{E_{11}b^2h^3} = \frac{2G}{P} \tag{6b}$$

Consequently, by employing Eqs. (6a) and (6b), Eq. (5) transforms into:

$$\dot{G} = \frac{2G}{a}\dot{a} + \frac{2G}{P}\dot{P} \tag{7}$$

Eq. (7) offers an alternative method for determining the rate of change of the SERR. Instead of fitting the SERR itself over time and then differentiating, this approach involves computing the right part of Eq. (7). For determining both the crack tip velocity ($\dot{a}$) and the change in applied force over time ($\dot{P}$), the procedure involves fitting the a and P values over time, followed by subsequent differentiation of the derived equations.

In the present study, we revisit the energy dissipation methodology proposed by Pascoe et al. [44–46]. A key aim of our research is to extend the linear correlations established for fatigue crack growth experiments, when the dissipated energy per cycle is plotted against the crack growth rate. We aim to examine if this correlation applies not only to fatigue experiments but also in cases where constant opening rates are imposed. In this method, we utilize the measured forces and displacements to compute the system's total strain energy, U, as Eq. (8) dictates:

$$U = \frac{1}{2}P(\delta - \delta_0) \tag{8}$$

where P is taken as the maximum resultant force on the specimen, δ is the displacement, δ_0 is the displacement for zero force. This term excludes any initial non-linearities observed, taking into account only the linear part of the $P-\delta$ curve. Linear elastic behavior of the specimen is assumed. By measuring U at regular intervals during the experiment, the energy dissipation dU/dN can be determined assuming that the reduction between two consecutively measured total energy (U) values equates to the dissipated energy. An important feature of the energy dissipation approach is that it makes it possible to separately characterize the resistance to crack growth, and the energy available for crack growth [46]. The resistance to crack growth, G^*, was defined in [31], as:

$$G^* = \frac{1}{b}\frac{dU/dN}{da/dN} = \frac{1}{b}\frac{dU/dt}{da/dt} \tag{9}$$

2.4. Fitting procedures

To calculate both the velocity of the crack tip and the change of applied load over time, the parameters measurements a and P, were plotted against time measurements, t. A two-term power equation of the form $a = kt^q + r$ provided the best results and was thus selected for fitting the results. The velocity of the crack tip and change of applied load over time is acquired by differentiation of the fitted $a(t)$ equations as $\dot{a} = kqt^{q-1}$. For fatigue, cycles N, were converted to time through the loading frequency f i.e., $t = N/f$.

3. Results

3.1. Similitude via the applied work

Alderliesten in [16], advocates for the use of the dissipated energy per cycle as a key factor in drawing conclusive insights for applying similitude in the context of fatigue crack growth. Employing this approach, visualized through Eq. (9), interesting linear correlations are unveiled. These correlations emerge when the rate of change of the dissipated energy, dU/dt, is plotted against the velocity of the crack tip, da/dt, with a focus on fatigue experiments (Fig. 2a). $G^* = dU/dA$, emerges as the slope of this linear correlation, passing through the origins of the axes, representing an average SERR value of the material tested. At this point it is noted here that dU/dA or $\frac{1}{b}\frac{dU/dt}{da/dt}$ corresponds to a mean SERR value and is not related to either $\Delta\sqrt{G}$, or ΔG for fatigue as discussed in [31]. The maximum SERR value achieved inside a fatigue loading cycle, G_{max}, commonly employed to communicate fatigue experiment outcomes, has been observed to exhibit a linear correlation with G^* in previous studies [29,31,32]. It is important to note, however, that this correlation does not imply the equivalence or coincidence of G^* and G_{max}. Fig. 2a illustrates the revealed linear correlation between the rate of change of the energy dissipated versus the crack tip velocity for the fatigue experiments using the CFRP material system. Although the results show evidence of a strong linear correlation, previous studies [27,30] reported that the slope's value is not consistent throughout the entire test and may undergo slight changes. Increase of the bridging zone length moves curves to the right part of the graph as also reported in [30]. Due to the release of strain energy as the crack length increases, the derivative of the strain energy with respect to time is negative. However, the values are presented here in absolute terms. To further investigate the linear correlation observed in fatigue results, the COR tests are represented in the same way in Fig. 2b. Evidently, a linear correlation also holds for COR tests. However, it is noteworthy that a different line is obtained compared to that observed in fatigue experiments, along with a notably higher R^2 value. It has to be stressed that the experimental data are fitted in lines of the type $y = ax$ with the slope having a dimension of $1/G^*$ (see Eq. (9)). Observing Fig. 2a and b we deduce that, depending on the load application method and bridging zone, upper and lower limits exist for the velocity of the crack tip. These velocities are delineated by two lines, forming a specific range of values within which the material can exhibit its average SERR or G^* values. Apparently, deriving a single average SERR value to describe the material's delamination under an arbitrary mode-I loading is not appropriate. To illustrate this more clearly, we plot both COR and AOR test results of the CFRP material system in Fig. 2c where a range of slopes representing average SERR values is extracted depending on the load application method and bridging zone. Examining Fig. 2c, it can be deduced that the two lines delineating the measured range could represent upper and lower average resistance limits of the material tested. For both COR and AOR tests the velocity of the crack tip changes from higher values (low bridging zones) to lower ones (high bridging zones) inversely proportional to the average SERR G^*. It seems that under displacement control fatigue experiments conducted at greater initial crack lengths and thus bridging zones, dU values decrease at a slower rate than dA values, signifying a greater resistance to crack

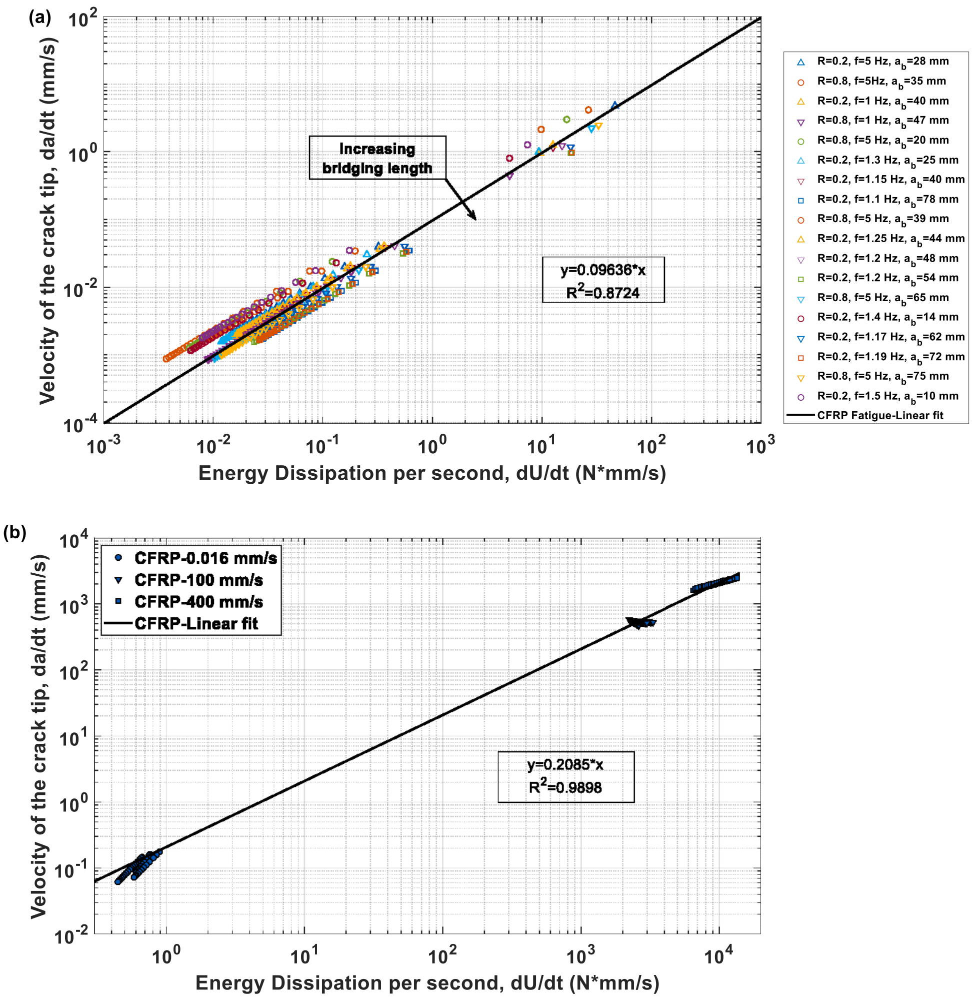

Fig. 2. Logarithmic scale. Comparison between the total dissipated energy per second with the velocity of the crack tip. (a) Results of the CFRP fatigue experimental campaign representing AOR tests (a_b: bridging zone length). (b) Results of the CFRP COR tests. (c) Comparison between CFRP AOR and COR tests results. (d) Results of the GFRP COR tests.

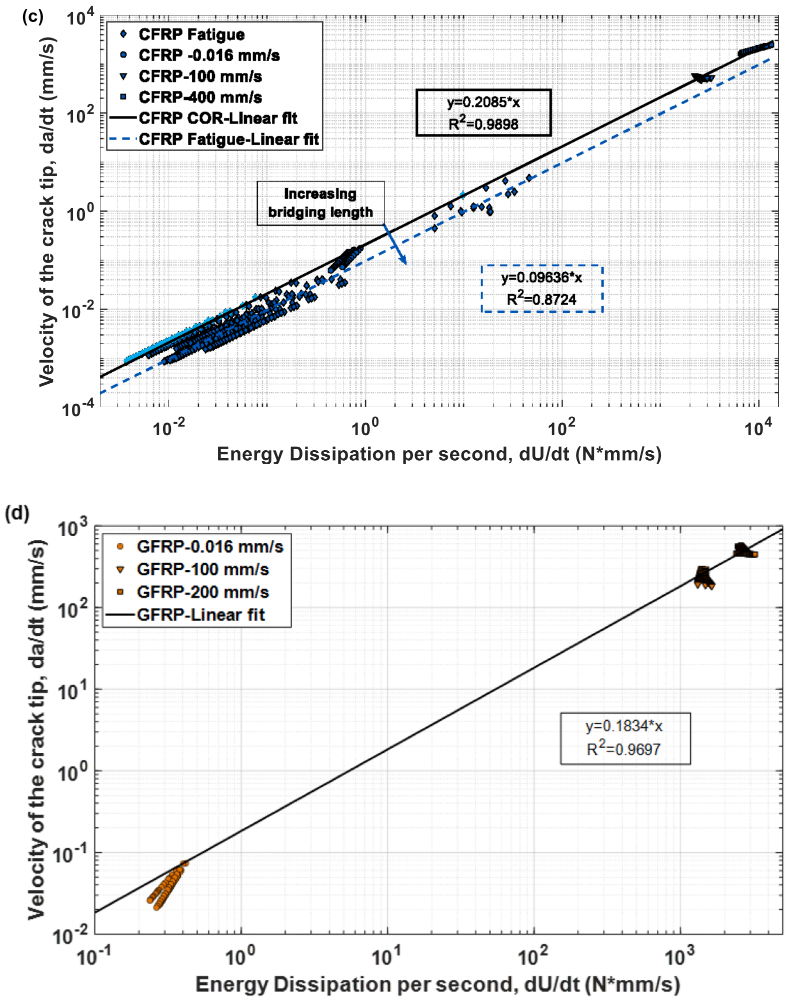

Fig. 2. (*continued*).

evolution. As a result, G^{*}, serving as a measure of average resistance to crack propagation regardless of load application, increases. A comparable pattern among data points was also reported in [27], where the analysis incorporates data from fatigue and quasi-static loading. In that study, quasi-static data points align with a lower slope compared to fatigue data indicating $G^{*}_{Q.S.} \geq G^{*}_{AOR}$. The effect of the stress ratio was examined however, the extent to which multiple bridging zones affect the aforementioned relation was not investigated. In our case, when all the results are plotted separately, a discernible distinction in slopes also emerges, however generally indicating $G^{*}_{COR} \leq G^{*}_{AOR}$ and thus $G^{*}_{Q.S.} \leq G^{*}_{AOR}$. The reasoning behind this inverse result is that all fatigue experiments that are conducted for the present work feature a minimum bridging zone of at least 10 *mm*, determined from prior quasi-static tests. This means that fatigue experiments commence at a minimum crack length of 60 *mm* (including a 10 *mm* bridging zone), while COR tests are introduced for testing at an initial crack length of 50 *mm* (without a bridging zone initially). Nevertheless, even when we restrict the comparison to only quasi-static and fatigue data in our case, there are datapoints (highlighted in pale blue in Figs. 2c and 3) that replicate the observed in [27] behavior. To sum up we deduce that the quasi-static G^{*} values can vary, being either greater or smaller than the fatigue G^{*} values, depending on the length of the bridging zone used in the fatigue experiment. In the present work, the conversion of loading cycles to time allows for a straightforward comparison between various experiment types without making any assumptions on the increments of damage evolution of COR tests. In [27], the authors developed a methodology to process quasi-static data in terms of loading cycles, facilitating comparison between fatigue and quasi-static loading. In this context, we augment the existing findings by incorporating data from high-speed loading, employing similar analysis. The results demonstrate that upper and lower average resistance limits exist for the material tested, established when both COR and AOR tests are included in the same graph. In the case of COR tests, increase of the loading rate leads to minor deviations of the slope's value. This suggests that, up to that specific rate, the average resistance of the material is almost irrespective of the loading rate employed in the experiment. It should be marked that due to the way the axes are shown, the upper limit corresponds to lower G^{*} values.

Fig. 2d illustrates the relationship between the crack tip velocity and the total dissipated energy per second for the GFRP material system. However, in this case, data from the literature [35] were exclusively available for COR tests, and as such, the comparison will be limited to the corresponding COR tests of the CFRP material system. The presence of a linear correlation is verified for the GFRP material system as well. The slope value at which the data points converge is lower than that observed in the CFRP material system, indicating that interlaminar crack propagation may occur at a faster rate in the CFRP specimens compared to the GFRP specimens.

3.2. A new approach to apply similitude

3.2.1. Paris-like description

The preceding section focused on revisiting the methodology initially introduced in [31], but trying to put both COR and AOR tests results under the same framework, in an attempt to characterize the mode-I crack growth independently of the loading rate/type. The correlation presented above was established between the velocity of the crack tip and the energy dissipation per second whereas the relevant literature tries persistently to connect the velocity of the crack tip with the SERR usually through variations of the Paris law. In this section, we will employ a similar analysis utilizing the SERR instead of the strain energy, towards a unifying description of mode-I interlaminar fracture in layered materials. First, we emphasize the known limitation to describe all the available experimental data utilizing a conventional Paris-like description which relates a form of SERR, e.g. G_{max}, with the crack growth rate, da/dN. The Paris relation as described in Eq. (1) is applied utilizing da/dt instead of da/dN to accommodate under the same description the COR tests as well, to investigate if all mode-I interlaminar fracture tests can be described in a unique -material dependent- manner.

Fig. 3 presents all the available experimental data (from two material systems) in terms of crack tip velocity versus G_{max} in the Paris law framework. Utilization of the maximum SERR, G_{max}, in the case of AOR tests, allows for a straightforward comparison with the COR counterparts. Evidently, the data are uncorrelated and there is no uniform description. If either ΔG or $\Delta\sqrt{G}$ are utilized in the Paris law insignificant changes arise. A large scatter of the data from fatigue tests is observed since the stress-ratio, fiber bridging and/or frequency effects expose the inability of Paris relation to provide a unifying description of the experimental data. The crack tip velocity increases proportionally with the rising loading rate, a relationship that aligns with what is intuitively expected. However, for COR tests, it remains nearly constant under a given loading rate. Towards the end of each COR experiment, a small decrease in the velocity of the crack tip is observed when the bridging zone is extended. In the case of AOR tests, deducing a singular initiation or threshold SERR value for the specific material through the Paris' framework proves challenging, as stress-ratio and fiber bridging significantly influence these values. Furthermore, for the COR test campaign, it is evident that the SERR generally decreases with a rising loading rate, visualized through an increasing velocity of the crack tip. This observation aligns with the findings of previous studies [26,34].

3.2.2. Rate of change of the SERR as a similitude parameter

Inspired by Eq. (7) we utilize the rate of change of the SERR as a candidate similitude parameter. Fig. 4a illustrates the correlation between the velocity of the crack tip and the rate of change of the SERR, for the AOR test campaign of CFRP specimens. Notably, a strong linear correlation is evident in this case, displaying a higher R^2 value compared to the value obtained in Fig. 2a, where the velocity of the crack tip is plotted against the rate of change of the dissipated energy. The effect of the bridging zone, observed in

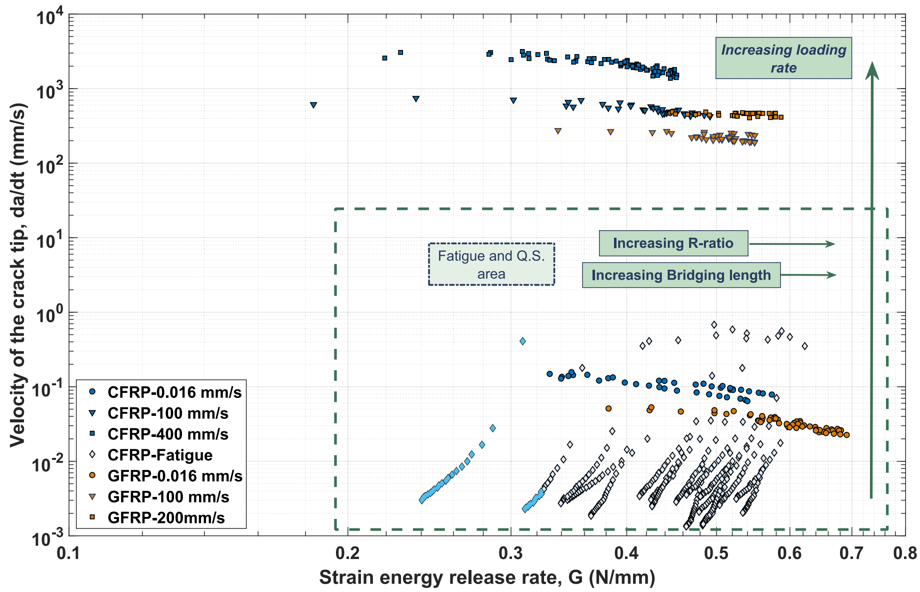

Fig. 3. Results of the experimental campaign when data from all experiments act as inputs in Paris' equation (Eq. (1)). In the case of fatigue testing G_{max} is utilized as the appropriate parameter for comparison.

Fig. 2a, appears to have no influence within the current description. Remarkably, the main factors affecting the Paris-like description of interlaminar fracture as demonstrated in Fig. 3 -such as stress ratio, frequency, and the bridging zone- do not show a significant influence with the new description. The authors acknowledge that experimental conditions can indeed impact fatigue delamination tests. However, utilizing equations misaligned with physics principles does not allow a unifying interpretation of test data. Specifically, the authors believe that frequency and stress ratio have a significant impact on fatigue delamination tests. The stress ratio dictates the amplitude of the oscillation, while the stress ratio, along with the frequency, determines the velocity of the oscillation and, consequently, the loading rate. The influence of these parameters on the loading rate gives rise to discrepancies in terms of both the SERR, as loading rate affects its values, and velocity of the crack tip, especially during the initial loading cycles. In Fig. 4b, the results of COR tests for the CFRP material system are presented. A strong linear correlation exists as well, with a similar R^2 value to the corresponding one in Fig. 2b. We have to stress the fact that all data shown in Fig. 4 are fitted to a $y = ax$ type of line since, intuitively for $\dot{G} = 0$ the crack tip velocity has to be zero. The data points align along a different line of higher slope compared to that of the AOR tests. We support that these two slope values delineate the velocity boundaries which an interlaminar crack is allowed to achieve under any mode-I loading in the specific material, as illustrated in Fig. 4c. Moreover, it is apparent that, when testing under CORs, the extracted slope value is higher than that obtained from AORs. The collapsing of the data points into two separate slopes is due to the fitting procedures, which smooth out fluctuations observed in the raw data. If someone measured the differentials as finite differences (e.g. $\Delta a/\Delta t$) the entire range would be covered with datapoints instead of the boundaries of the range. The nearly perfect alignment of the COR tests datapoints, while using a power equation for the fitting procedure, is rational, due to the nature of constant/monotonic load application. However, concerning AOR tests, it is the authors' perspective that, in reality, the positioning of data points, particularly

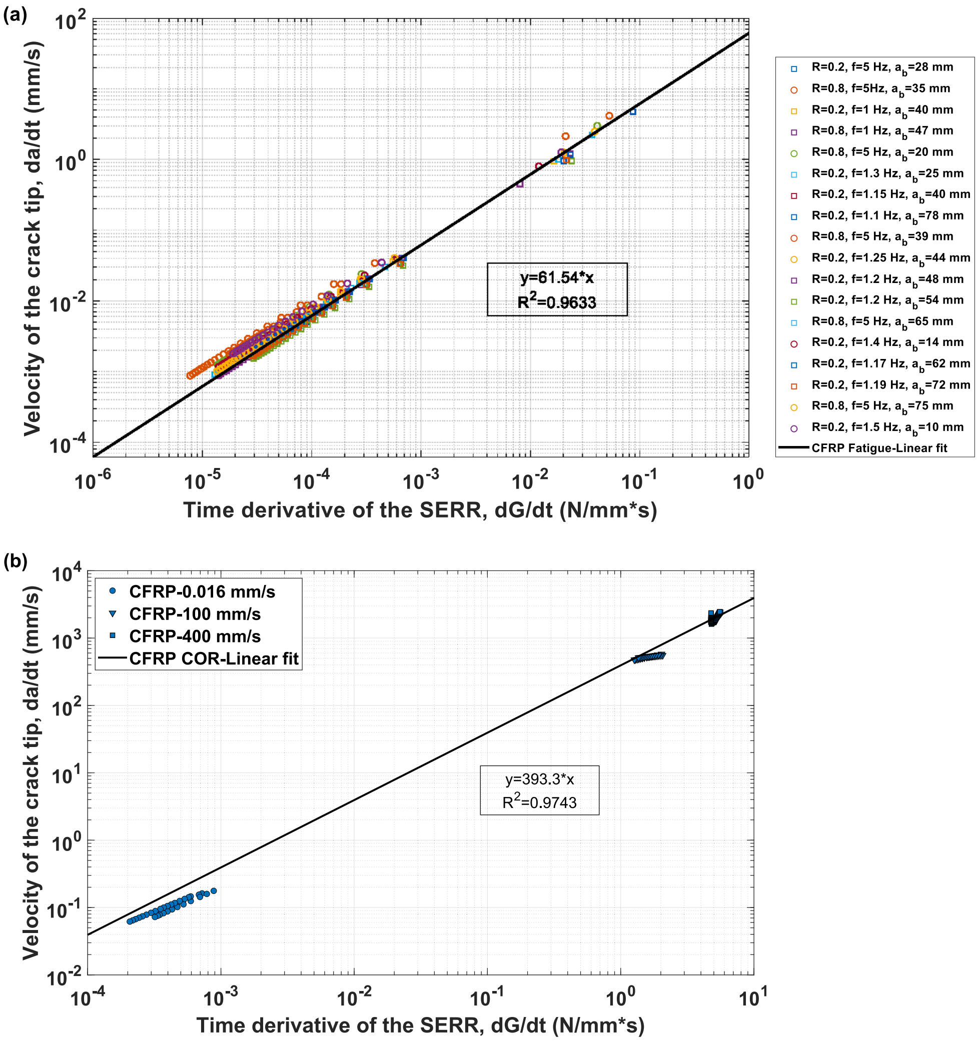

Fig. 4. Logarithmic scale. Comparison between the change rate of the SERR with the velocity of the crack tip. (a) Results of the CFRP fatigue experimental campaign representing AOR tests (a_b: bridging zone length). (b) Results of the CFRP COR tests. (c) Comparison between CFRP AOR and COR tests results. (d) Results of all the available data including both CFRP and GFRP material systems.

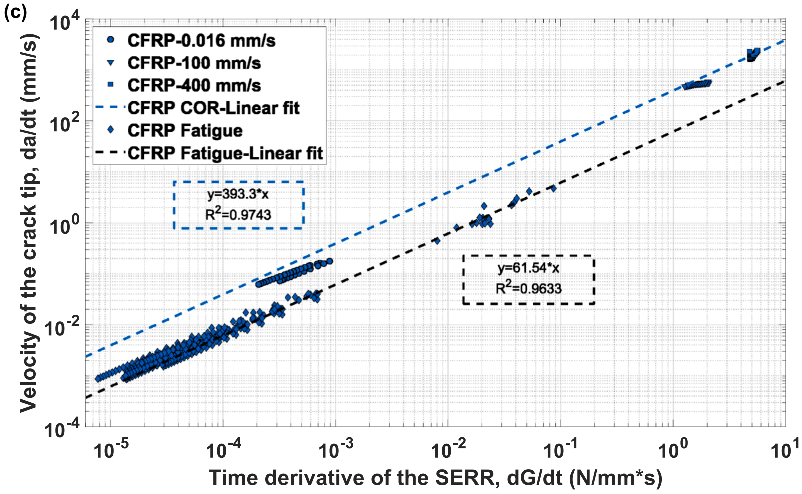

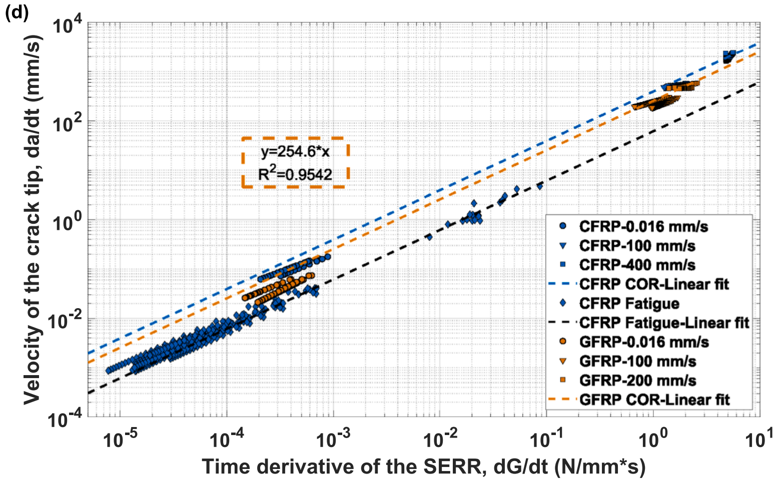

Fig. 4. (*continued*).

those corresponding to the initial cycles of loading, is highly dependent on how the loading rate is applied. As mentioned in previous sections, the AOR tests are conducted through displacement control fatigue experiments and thus load application is determined by the maximum displacement value, δ_{max}, imposed. However, for each crack increase, there exists a corresponding δ_{crit} value, signifying the initiation of the crack. Consequently, we categorize fatigue loading into two distinct scenarios within the framework of Fig. 4c:

i. $\delta_{max} \geq \delta_{crit}$: If the value of δ_{max} applied is equal to or greater than the δ_{crit} value corresponding to a given crack length, then the initial cycle of AOR loading will mimic the COR fracture behavior. Consequently, the first cycle data points will align with the slope of the COR tests. Depending on the extent of the difference between the value of δ_{max} and δ_{crit}, we obtain data points with higher velocities and change rates of SERR, while still following the same COR-determined slope. Potential acceleration effects might affect initial values. Data points extracted from the analysis of later cycles of loading will gradually converge toward the slope extracted from AOR tests.
ii. $\delta_{max} < \delta_{crit}$: If the value of δ_{max} applied is lower than the δ_{crit} value corresponding to a given crack length, the initial cycle data points will fall within the range created by the slopes of COR and AOR tests. Data points extracted from the analysis of later cycles of loading will, once again, gradually converge toward the slope extracted from AOR tests.

From the above statements, we conclude that the upper boundary as marked from the COR tests can serve as an initiation slope from which value and above the specimen always initiates and propagates cracks and the lower boundary extracted from AOR tests that could serve as a threshold slope from which value and below the specimen never initiates and propagates cracks. Thus, during interlaminar fracture, the velocity of a crack tip is constrained depending on the material/interface through which it propagates. This is mathematically described as:

$$C^{*}_{AOR}\dot{G} \leq \dot{a} \leq C^{*}_{COR}\dot{G} \tag{10a}$$

$$c^*_{COR}\dot{a} \leq \dot{G} \leq c^*_{AOR}\dot{a} \tag{10b}$$

Where C^*_{COR} and C^*_{AOR} are the values of the corresponding slopes and $c^* = 1/C^*$. The slopes extracted in Fig. 2 represent average SERR values as the units of measurement dictate. When examining Fig. 4, a pertinent question emerges: What do these slopes signify? According to Eqs. (10a) and (10b) the constants c^*_{COR} and c^*_{AOR} have units of $\frac{J}{m^3}$ or $\frac{N}{mm^2}$ i.e. MPa similar to the $\frac{\partial G}{\partial a}$ term presented in Eq. (5), and thus, they could be physically understood as stresses representing initiation and threshold values, potentially suggesting a more representative fracture toughness property rather than G or K or an additional property of fracture that remained unexplored. The proposed new interpretation of mode-I interlaminar fracture in layered materials suggests a consistent combination of both average SERR and stress values, unaffected by the loading rate, stress ratio, and bridging zone effects. It seems that the only parameter affecting the constants of Eqs. (10a) and (10b) is the way the mode-I loading is applied. In Fig. 4c, AOR datapoints collapse on a lower slope, representing higher stress values than the COR datapoints ($c^*_{AOR} > c^*_{COR}$). However, as mentioned above, equality of these terms is possible. Fig. 4d mirrors Fig. 4c but also incorporates data points from the COR tests of GFRP specimens. Clearly, GFRP COR tests data points align at a slope of lower value compared to the collapse of CFRP COR tests data points meaning that the GFRP material system demonstrates increased fracture toughness when compared to the CFRP material system. This is clearly observable through the corresponding average SERR, G^*, or SERR, G, values presented in Figs. 2 and 3 respectively.

4. Discussion

While interlaminar fatigue fracture has for over three decades been studied with the empirical approach of Paris law-like models, a fresh unified perspective verified on vast experimental evidence from two material systems suggests that the velocity of the crack tip, $\dot{a}$, is linearly correlated, through a material specific range of slopes to both the energy dissipation per second, i.e., the $\dot{U}$, and the rate of change of the SERR, i.e., the $\dot{G}$, unaffected by parameters such as loading rate or type, stress ratio, bridging zone and frequency. These linear correlations are characterized by slopes that signify average SERR and novel average stress values respectively. Within the framework of this new interpretation of mode-I interlaminar crack propagation, it seems that the only parameter influencing the fracture behavior of the specimens tested is the method of load application, adjusting the response of the specimen in terms of crack velocity, within a material/interface dependent specific range.

The robust linear correlation observed for COR tests holds significant implications. If this correlation remains consistent and is verified by other researchers as well, it could allow us to extrapolate crack tip velocities in experiments with different loading rates using data from a single loading rate test. This has the potential to reduce the number of overall experiments required to characterize the mode-I delamination of a layered material reducing associated costs. This physically consistent new equation successfully describes data from several fracture tests under quasi-static, dynamic, low or high loading rates, since the fracture behavior of a material seems to be governed by a material specific range of slopes. Integrating laboratory data under a variety of test conditions into the simple and unifying formulation presented above reveals a strong correlation and enables a new understanding of the mode-I interlaminar fracture without the problems induced by the state-of-the-art empirical models.

Another crucial aspect of the present findings is the novelty of the stress term 'c^*' in Eq.(10b) extracted from the above analysis. The authors believe that this discovery charts a course beyond existing literature and underscores the importance of continually reevaluating established frameworks. Unlike previous works that focus on fatigue initiation and threshold values of the SERR, and initiation and propagation values of the SERR for COR tests, this finding provides initiation and threshold values that are not contingent on experimental conditions but are instead specific to the material, expressed in terms of both SERR and stress. This unified perspective gives a new interpretation of experimental evidence opening new avenues in the understanding of interlaminar fracture related phenomena not only in layered composite materials but potentially in other material classes as well.

5. Conclusions

In this study, we have presented a comprehensive analysis of the fracture phenomenon, supported by vast experimental evidence extracted from various fatigue, quasi-static, and high-speed mode-I fracture tests. The conversion of loading cycles, N, into time, s, facilitated a direct comparison of mode-I crack extensions under the whole spectrum of loading conditions. A physically meaningful SERR can be consistently derived from a plot of crack velocity versus rate of change of dissipated energy, confirming and expanding upon previous literature findings. The average SERR, G^*, calculated through energy balance principles, serves to characterize both AOR and COR crack extensions. The velocity of the crack tip for both COR and AOR tests gradually shifts from high (low bridging zone) to low (high bridging zone), inversely proportional to the average SERR or material resistance. The exploration of potential linear correlations governing the tested materials involved utilizing the chain differentiation of the SERR. This approach suggested a new linear correlation between the rate of change of the SERR and the velocity of the crack tip. The introduction of novel stress terms has allowed us to unravel previously unexplored facets of the fracture process, suggesting a potentially more appropriate description of a material's fracture toughness or an additional property of fracture. The lower limit, established once again by AOR testing under fatigue loading, concerns the lowest crack velocity values, while the upper limit for the velocity, determined by COR testing encompassing quasi-static and high-speed loading, held true regardless of the loading rate imposed. It becomes evident that the load application governs the fracture response of the tested specimens, providing insights into the materials themselves, as distinct slopes emerged for the two materials under examination. Consequently, these robust linear correlations suggest that the maximum/minimum velocity of a developing crack within a material is contingent on the material's intrinsic properties. These correlations identify initiation, propagation and threshold values that are independent of experimental conditions and specific to the material, expressed in terms of both SERR and stress. Within the tested rates, a material's fracture toughness does not appear to be significantly influenced by the loading rate imposed, stress ratio or frequency chosen and existing bridging zone but is strongly linked to the method of load application, shaping the fracture behavior of the material in between AOR and COR testing.

CRediT authorship contribution statement

Lucas Adamos: Writing – original draft, Visualization, Methodology, Investigation, Formal analysis, Data curation, Conceptualization. **René Alderliesten:** Writing – review & editing, Visualization, Supervision, Resources, Conceptualization. **Theodoros Loutas:** Writing – review & editing, Visualization, Supervision, Resources, Funding acquisition, Conceptualization.

Declaration of competing interest

The authors declare that they have no known competing financial interests or personal relationships that could have appeared to influence the work reported in this paper.

Data availability

Data will be made available on request.

Acknowledgements

Mr. Lucas Adamos is financially supported by Grant 80676 from the Research Committee of the University of Patras via C. CARATHEODORI program. Part of this publication is based upon work from COST Action (CA18120), supported by COST (European Cooperation in Science and Technology).

Appendix A. . Supplementary Figure

In response to the reviewer's request, Fig. A1 illustrates the complete loading history obtained from experiments conducted under the two different stress ratios used in this study. To avoid overwhelming the reader, we've included one representative hysteresis loop for each case, rather than presenting the full load histories for all 18 fatigue experiments. Fatigue data will be provided upon request.

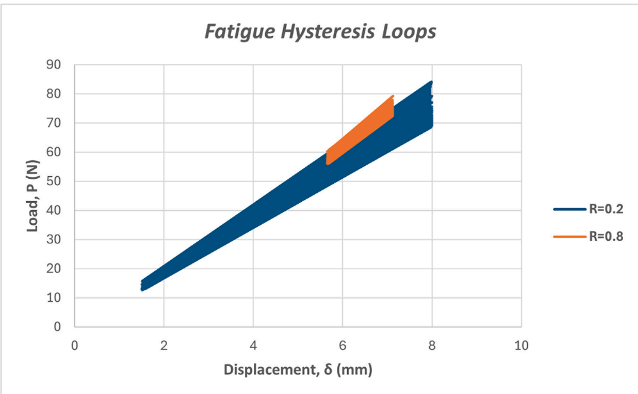

Fig. A1. Fatigue hysteresis loops extracted from experiments conducted under the two stress ratios used.

References

[1] Paris P, Gomez MWA, Paris PC, Gomez MP, Anderson WEP. A rational analytic theory of fatigue. Trend Eng 1961;13:9–14.
[2] Paris CP. The fracture mechanics approach to fatigue. Fatigue-An Interdiscip Approach 1964.
[3] Hartman A, Schijve J. The effects of environment and load frequency on the crack propagation law for macro fatigue crack growth in aluminium alloys. Eng Fract Mech 1970;1:615–31. https://doi.org/10.1016/0013-7944(70)90003-2.
[4] Jones R, Pitt S, Bunner AJ, Hui D. Application of the Hartman-Schijve equation to represent Mode I and Mode II fatigue delamination growth in composites. Compos Struct 2012;94:1343–51. https://doi.org/10.1016/j.compstruct.2011.11.030.
[5] Jones R, Stelzer S, Brunner AJ. Mode I, II and Mixed Mode I/II delamination growth in composites. Compos Struct 2014;110:317–24. https://doi.org/10.1016/j.compstruct.2013.12.009.

[6] Pascoe JA, Alderliesten RC, Benedictus R. Methods for the prediction of fatigue delamination growth in composites and adhesive bonds - a critical review. Eng Fract Mech 2013;112–113:72–96. https://doi.org/10.1016/j.engfracmech.2013.10.003.
[7] Allegri G, Jones MI, Wisnom MR, Hallett SR. A new semi-empirical model for stress ratio effect on mode II fatigue delamination growth. Compos Part A Appl Sci Manuf 2011;42:733–40. https://doi.org/10.1016/j.compositesa.2011.02.013.
[8] Allegri G, Wisnom MR. A non-linear damage evolution model for mode II fatigue delamination onset and growth. Int J Fatigue 2012;43:226–34. https://doi.org/10.1016/j.ijfatigue.2012.03.016.
[9] Pascoe J-A. Slow-growth damage tolerance for fatigue after impact in FRP composites: why current research won't get us there. Theor Appl Fract Mech 2021;116:103127. https://doi.org/10.1016/j.tafmec.2021.103127.
[10] Yao L, Sun Y, Guo L, Zhao M, Jia L, Alderliesten RC, et al. A modified Paris relation for fatigue delamination with fibre bridging in composite laminates. Compos Struct 2017;176:556–64. https://doi.org/10.1016/j.compstruct.2017.05.070.
[11] Blanco N, Gamstedt EK, Asp LE, Costa J. Mixed-mode delamination growth in carbon-fibre composite laminates under cyclic loading. Int J Solids Struct 2004;41:4219–35. https://doi.org/10.1016/j.ijsolstr.2004.02.040.
[12] Zambelis G, Da Silva BT, Klinkova O, Tawfiq I, Lanouette C. Evaluation of the energy release rate in mode I of asymmetrical bonded composite/metal assembly. Eng Fract Mech 2018;190:175–85. https://doi.org/10.1016/j.engfracmech.2017.12.007.
[13] Sousa JA, Pereira AB, Martins AP, de Morais AB. Mode II fatigue delamination of carbon/epoxy laminates using the end-notched flexure test. Compos Struct 2015;134:506–12. https://doi.org/10.1016/j.compstruct.2015.08.002.
[14] Zhang J, Peng L, Zhao L, Fei B. Fatigue delamination growth rates and thresholds of composite laminates under mixed mode loading. Int J Fatigue 2012;40:7–15. https://doi.org/10.1016/j.ijfatigue.2012.01.008.
[15] Rans C, Alderliesten R, Benedictus R. Misinterpreting the results: How similitude can improve our understanding of fatigue delamination growth. Compos Sci Technol 2011;71:230–8. https://doi.org/10.1016/j.compscitech.2010.11.010.
[16] Alderliesten RC. How proper similitude can improve our understanding of crack closure and plasticity in fatigue. Int J Fatigue 2016;82:263–73. https://doi.org/10.1016/j.ijfatigue.2015.04.011.
[17] Amaral L, Alderliesten R, Benedictus R. Understanding mixed-mode cyclic fatigue delamination growth in unidirectional composites: An experimental approach. Eng Fract Mech 2017;180:161–78. https://doi.org/10.1016/j.engfracmech.2017.05.049.
[18] Hojo M, Ando T, Tanaka M, Adachi T, Ochiai S, Endo Y. Modes I and II interlaminar fracture toughness and fatigue delamination of CF/epoxy laminates with self-same epoxy interleaf. Int J Fatigue 2006;28:1154–65. https://doi.org/10.1016/j.ijfatigue.2006.02.004.
[19] Jones R, Kinloch AJ, Hu W. Cyclic-fatigue crack growth in composite and adhesively-bonded structures: The FAA slow crack growth approach to certification and the problem of similitude. Int J Fatigue 2016;88:10–8. https://doi.org/10.1016/j.ijfatigue.2016.03.008.
[20] Hojo M, Tanaka K, Gustafson CG, Hayashi R. Effect of stress ratio on near-threshold propagation of delimination fatigue cracks in unidirectional CFRP. Compos Sci Technol 1987;29:273–92. https://doi.org/10.1016/0266-3538(87)90076-5.
[21] Yao L, Alderliesten RC, Benedictus R. Interpreting the stress ratio effect on delamination growth in composite laminates using the concept of fatigue fracture toughness. Compos Part A Appl Sci Manuf 2015;78:135–42. https://doi.org/10.1016/j.compositesa.2015.08.005.
[22] Shahverdi M, Vassilopoulos AP, Keller T. Experimental investigation of R-ratio effects on fatigue crack growth of adhesively-bonded pultruded GFRP DCB joints under CA loading. Compos Part A Appl Sci Manuf 2012;43:1689–97. https://doi.org/10.1016/j.compositesa.2011.10.018.
[23] Mall S, Ramamurthy G, Rezaizdeh MA. Stress ratio effect on cyclic debonding in adhesively bonded composite joints. Compos Struct 1987;8:31–45. https://doi.org/10.1016/0263-8223(87)90014-6.
[24] Hu W, Jones R, Kinloch AJ. Discussion of the Stress Ratio Effect on the Fatigue Delamination Growth Characterization in FRP Composite Structures. Procedia Struct Integr 2016;2:66–71. https://doi.org/10.1016/j.prostr.2016.06.009.
[25] Yao L, Sun Y, Zhao M, Alderliesten RC, Benedictus R. Stress ratio dependence of fibre bridging significance in mode I fatigue delamination growth of composite laminates. Compos Part A Appl Sci Manuf 2017;95:65–74. https://doi.org/10.1016/j.compositesa.2016.11.030.
[26] Ekhtiyari A, Alderliesten R, Shokrieh MM. Loading rate dependency of strain energy release rate in mode I delamination of composite laminates. Theor Appl Fract Mech 2021;112. https://doi.org/10.1016/j.tafmec.2021.102894.
[27] Amaral L, Yao L, Alderliesten R, Benedictus R. The relation between the strain energy release in fatigue and quasi-static crack growth. Eng Fract Mech 2015;145:86–97. https://doi.org/10.1016/j.engfracmech.2015.07.018.
[28] Yao L, Sun Y, Guo L, Lyu X, Zhao M, Jia L, et al. Mode I fatigue delamination growth with fibre bridging in multidirectional composite laminates. Eng Fract Mech 2018;189:221–31. https://doi.org/10.1016/j.engfracmech.2017.11.013.
[29] Pascoe JA, Zavatta N, Troiani E, Alderliesten RC. The effect of bond-line thickness on fatigue crack growth rate in adhesively bonded joints. Eng Fract Mech 2020;229. https://doi.org/10.1016/j.engfracmech.2020.106959.
[30] Yao L, Alderliesten RC, Zhao M, Benedictus R. Discussion on the use of the strain energy release rate for fatigue delamination characterization. Compos Part A Appl Sci Manuf 2014;66:65–72. https://doi.org/10.1016/j.compositesa.2014.06.018.
[31] Pascoe JA, Alderliesten RC, Benedictus R. On the physical interpretation of the R-ratio effect and the LEFM parameters used for fatigue crack growth in adhesive bonds. Int J Fatigue 2017;97:162–76. https://doi.org/10.1016/j.ijfatigue.2016.12.033.
[32] Usman M, Pascoe JA, Alderliesten RC, Benedictus R. The effect of temperature on fatigue crack growth in FM94 epoxy adhesive bonds investigated by means of energy dissipation. Eng Fract Mech 2018;189:98–109. https://doi.org/10.1016/j.engfracmech.2017.10.007.
[33] Pascoe JA, Alderliesten RC, Benedictus R. Characterising resistance to fatigue crack growth in adhesive bonds by measuring release of strain energy. Procedia Struct Integr 2016;2:80–7. https://doi.org/10.1016/j.prostr.2016.06.011.
[34] Ekhtiyari A, Shokrieh MM, Alderliesten R. Loading rate effects on mode-I delamination in glass/epoxy and glass/CNF/epoxy laminated composites. Eng Fract Mech 2020;228:106908. https://doi.org/10.1016/j.engfracmech.2020.106908.
[35] Ekhtiyari A (Amin). Loading rate effects on the Mode I delamination growth of laminated Glass/epoxy and Glass/CNF-modified epoxy DCB specimens 2019. https://doi.org/10.4121/UUID:1E7FE12A-C5A1-4840-A24C-2BA977783E1B.
[36] Ekhtiyari A (Amin). Loading rate effects on the Mode I delamination growth of laminated carbon/epoxy composite DCB specimens 2019. https://doi.org/10.4121/UUID:70505D03-0A81-4497-BA73-92A3B4563C2A.
[37] Liu H, Nie H, Zhang C, Li Y. Loading rate dependency of Mode I interlaminar fracture toughness for unidirectional composite laminates. Compos Sci Technol 2018;167:215–23. https://doi.org/10.1016/j.compscitech.2018.07.040.
[38] Kusaka T, Hojo M, Mai YW, Kurokawa T, Nojima T, Ochiai S. Rate dependence of mode I fracture behaviour in carbon-fibre/epoxy composite laminates. Compos Sci Technol 1998;58:591–602. https://doi.org/10.1016/S0266-3538(97)00176-0.
[39] Blackman BRK, Kinloch AJ, Paraschi M. The determination of the mode II adhesive fracture resistance, GIIC, of structural adhesive joints: An effective crack length approach. Eng Fract Mech 2005;72:877–97. https://doi.org/10.1016/j.engfracmech.2004.08.007.
[40] Brunner AJ, Blackman BRK, Williams JG. Calculating a damage parameter and bridging stress from GIC delamination tests on fibre composites. Compos Sci Technol 2006;66:785–95. https://doi.org/10.1016/j.compscitech.2004.12.040.
[41] de Moura MFSF, de Morais AB. Equivalent crack based analyses of ENF and ELS tests. Eng Fract Mech 2008;75:2584–96. https://doi.org/10.1016/j.engfracmech.2007.03.005.
[42] Madureira F, da Silva LFM, Tita V. Compliance Methods For Bonded Joints: Part I - Investigation Of The Standardized Methods To Obtain The Strain Energy Release Rate For Mode I. J Adhes 2022;00:1–22. https://doi.org/10.1080/00218464.2022.2144731.
[43] Qiao P, Chen F. On the compliance and energy release rate of generically-unified beam-type fracture specimens 2011;vol. 45. https://doi.org/10.1177/0021998310371545.

[44] Pascoe JA, Alderliesten RC, Benedictus R. On the relationship between disbond growth and the release of strain energy. Eng Fract Mech 2015;133:1–13. https://doi.org/10.1016/j.engfracmech.2014.10.027.

[45] Pascoe JA, Alderliesten RC, Benedictus R. Towards Understanding Fatigue Disbond Growth via Cyclic Strain Energy. Procedia Mater Sci 2014;3:610–5. https://doi.org/10.1016/j.mspro.2014.06.101.

[46] Pascoe JA, Alderliesten RC, Benedictus R. Characterising resistance to fatigue crack growth in adhesive bonds by measuring release of strain energy. Procedia Struct. Integr., vol. 2, Elsevier B.V.; 2016, p. 80–7. https://doi.org/10.1016/j.prostr.2016.06.011.